

QCD Phase Diagram and the Finite Volume Fireball: A Model Study

Adiba Shaikh^{a†}

Department of Physics, Indian Institute of Technology Bombay, Powai, Mumbai 400076, India.

Ranjita K. Mohapatra[‡]

Department of Physics, Rajdhani College, Bhubaneswar, Odisha 751003, India.

Saumen Datta[§]

Tata Institute of Fundamental Research, Homi Bhabha Road, Mumbai 400005, India.

Experimental investigations of the phase diagram of strongly interacting matter involve collisions of heavy ions at ultrarelativistic velocities. The medium created in such a collision is often of dimensions a few fermi, in particular in the Beam Energy Scan experiments. An understanding of the effect of the finite volume and the boundary is important for connecting the experimental results to the phase diagram.

Using the Nambu Jona-Lasinio model, an effective theory for the chiral transition of quantum chromodynamics (QCD), we have studied the effect of the finite volume of the fireball on the transition line at finite temperature and density using the MIT boundary condition to mimic the condition that the system is deconfined inside. We studied the effect of the finite volume on the transition temperature and on number density and its susceptibilities. The volume effects should be considered when looking for signatures of the phase diagram in experiments.

Keywords: Finite volume, QCD phase diagram, NJL model, MIT boundary condition.

I. INTRODUCTION

The bulk property of the strongly interacting matter has been the subject of detailed experimental investigation in recent times [1–4]. Strongly interacting matter is expected to manifest itself in a deconfined, chiral symmetry-restored phase, called the quark-gluon plasma (QGP), at very high temperatures [5, 6]. Experimentally, this phase has been explored in the study of the medium created in the collision of heavy ions at ultrarelativistic velocities, in particular in the Relativistic Heavy Ion Collider (RHIC) in BNL, USA [3] and the Large Hadron Collider (LHC) in CERN, Geneva [1]. The phase structure at high number density is being explored in the Beam Energy Scan (BES) experiments in RHIC [4] and will be further explored in future experiments in NICA, JINR [7] and in the CBM experiment in FAIR [8]. The knowledge about the phases at high density is complemented by the data from neutron stars and their mergers [9]. On the theory side, the properties of the deconfined state at high temperatures are well-understood from large-scale numerical studies of quantum chromodynamics (QCD), the theory of strongly interacting matter, using lattice discretization [5]. Lattice studies are more difficult at nonzero baryon number chemical potential (μ_B); however, the equation of state and baryon number susceptibilities have been calculated at large temperatures and moderate values of μ_B . At higher values of μ_B , or lower temperatures, one has to rely on QCD-based models [10, 11].

The theoretical studies, in particular the lattice-discretized QCD (LQCD) studies are for static equilibrated infinite volume systems. On the other hand, the medium created in RHIC and LHC experiments is rapidly evolving, and the system size is not too large. In particular, in the BES studies the system dimension can be a few fermi, not too large compared to the typical correlation length in strong interaction physics. The current experimental efforts are to study QGP in smaller systems. All this makes an understanding of the volume effect important.

In this paper, the aim is to get an idea of the effect of the finite volume on the phase diagram for a static system; the effects of the dynamic nature is being left for a future study. We study the phase diagram using the Nambu Jona-Lasinio (NJL) model [10], which is an effective model expected to capture the physics related to the chiral symmetry, in particular, the spontaneous chiral symmetry breaking. Since the finite temperature crossover is associated with the melting of the chiral condensate, the NJL model is expected to capture the basic features of the crossover.

In a study of the finite volume effects it is essential that realistic boundary conditions are put in for the system. The actual boundary of the medium created in the heavy ion collision experiments is of complicated

^a Current affiliation: *Tata Institute of Fundamental Research, Homi Bhabha Road, Mumbai 400005, India.*

[†] adibashaikh9@gmail.com

[‡] ranjita.iop@gmail.com

[§] saumen@theory.tifr.res.in

geometry. We take the simplified MIT boundary condition on a spherical geometry [12] (see [13] for a pedagogic discussion). While simple, the MIT boundary condition captures the essential physics that inside the boundary we have a deconfined medium. The spherical MIT bag model has been used to study the effect of the finite size of the QGP droplet on the thermal phase-space distributions of quarks and gluons [14].

The effect of the finite volume on the chiral transition has been studied before [15–23]. These studies have used the anti-periodic (APBC) and periodic (PBC) boundary conditions, or have put in a lower cutoff in momentum. However, these boundary conditions do not mimic a finite-volume fireball; they are boundary conditions used in theoretical studies to mimic an infinite-volume system within a finite-volume setup, e.g., in numerical lattice studies. In Appendix B we compare the MIT boundary condition results with those obtained with other boundary conditions. The MIT boundary condition has been used before, for studying the chiral crossover at $\mu_B = 0$ on a sphere [24], and for a rotating fermionic system in a cylinder [25, 26]. Here we use it to study the phase diagram in the (T, μ_B) plane and the baryon number susceptibilities.

The plan of the paper is as follows. In Section II we outline the basic calculations, discuss the boundary conditions, and specify the parameters used. The change of the phase diagram with changing volume is discussed in Section III. The number density and the susceptibilities in the critical region are discussed in Section IV. We summarize our results in Section V. The relevant equations for the MIT boundary condition and other details are compiled in Appendix A. Appendix B has a discussion of other boundary conditions.

II. FORMALISM AND THE BOUNDARY CONDITION

The NJL model is an effective model of the spontaneous chiral symmetry breaking of QCD [10, 27]. The degrees of freedom are only quarks; the effects of the gluonic interactions are included in four-fermion interaction terms, chosen such that the Lagrangian is chirally symmetric.

We will work with the two-flavor, isospin symmetric theory. The NJL Lagrangian for two degenerate flavors of light quarks is,

$$\mathcal{L}_{\text{NJL}} = \bar{\psi}(i\gamma_\mu \partial^\mu - \hat{m})\psi + G [(\bar{\psi}\psi)^2 + (\bar{\psi}i\gamma_5\bar{\tau}\psi)^2], \quad (1)$$

where $\psi = \begin{pmatrix} \psi_u \\ \psi_d \end{pmatrix}$ is the quark field, $\hat{m} = \text{diag}(m, m)$ is the degenerate light quark mass matrix, and G is the coupling strength of the effective four-fermion interaction between quarks. In the massless limit ($m = 0$), \mathcal{L}_{NJL} has a global $SU(2)_L \times SU(2)_R \times U(1)_V$ symmetry. This symmetry is spontaneously broken to $SU(2)_V \times U(1)_V$ as the chiral condensate $\langle\bar{\psi}\psi\rangle$ takes a nonzero value. In the presence of the mass term, the symmetry is also explicitly broken, leading to a preferred vacuum in the broken phase.

We will be studying the theory in the mean-field (MF) approximation. Writing the chiral condensate to be:

$$\langle\bar{\psi}\psi\rangle = -\frac{\sigma}{2G}, \quad (2)$$

\mathcal{L}_{NJL} can be rewritten in the mean-field approximation as,

$$\mathcal{L}_{\text{NJL}}^{\text{MF}} = \bar{\psi}(i\gamma_\mu \partial^\mu - M)\psi - \frac{\sigma^2}{2G}, \quad M = m + \sigma. \quad (3)$$

Then the effective potential is given by,

$$V_{\text{eff}}(\sigma) = -\frac{1}{V} \log Z = \frac{\sigma^2}{2G} - \int \mathbb{D}p \log \det(\gamma \cdot p - M), \quad (4)$$

and σ can be obtained from the minimum of $V_{\text{eff}}(\sigma)$: $\frac{\partial V_{\text{eff}}}{\partial \sigma} = 0$. Here $\mathbb{D}p$ refers to the regularized momentum integral.

The four-fermion term in \mathcal{L}_{NJL} makes the theory non-renormalizable. Hence, a suitable regularization method has to be specified, and the results will depend on the regularization parameter. We have used Schwinger's proper time regularization [27, 28], with the cutoff $\tau_{\text{UV}} = 1/\Lambda_{\text{UV}}^2$. Therefore, our model has three parameters: m, G and the UV momentum cutoff Λ_{UV} . These parameters can be chosen by specifying the pion mass, the pion decay constant and either the chiral condensate or the chiral transition temperature (T_χ). Some suitable parameter sets, and how they affect the chiral crossover temperature, have been discussed in Ref. [28]. The phase diagram can be qualitatively different for the different parameter sets. In particular, for some choices of parameters one gets a critical point and a first-order transition at large quark number chemical potential $\mu = \frac{\mu_B}{3}$, while for some other choices, the transition is a crossover in the whole (T, μ) plane. We have chosen the following parameter set:

m (MeV)	G (GeV $^{-2}$)	Λ_{UV} (MeV)
15	17.2	645

This parameter set was already explored in Ref. [28]. It has a first-order transition line at large μ , ending at a critical point at $\mu_c \approx 340$ MeV. At $\mu = 0$, it shows a chiral transition at $T_\chi \approx 186$ MeV. These values are larger than those expected for QCD: lattice calculations find $T_\chi \approx 156$ MeV[29], and estimates of $\mu_{q,c}$, while less certain, indicate values < 200 MeV [30]. Here our aim is not to tune the absolute value of these parameters but to look at their variation with the system size.

We will be studying the system at finite temperature T and quark number chemical potential μ . μ is introduced by adding $\mu\psi^\dagger\psi$ to Eq. (1). To get the thermodynamic potential, the integral over p_0 in Eq. (4) has to be turned into a fermionic Matsubara sum. For finite volume, the integral over spatial momenta, $\frac{d^3 p}{(2\pi)^3}$, will be replaced by a sum over the momentum modes allowed by the boundary condition. For a study of the effect of finite volume, imposing a proper boundary condition is important. As we discussed in Section I, the exact boundary condition for the medium created in RHIC or LHC is complicated; because it is time-dependent and also changes from event to event. Since we are only interested in getting an idea about how different the finite volume system can be from an infinite volume system, we will take a simple spherical geometry. The important physics that we want to capture is that the deconfined QGP is only contained within this geometry. For this, we impose the MIT boundary condition, which implies that the normal component of the quark current becomes zero at the boundary. More precisely, we impose the boundary condition [12, 13],

$$(-i\hat{r} \cdot \gamma)\psi(t, r, \theta, \phi)|_{r=R} = \psi(t, r, \theta, \phi)|_{r=R}, \quad (5)$$

where \hat{r} is the unit vector normal to the spherical surface and γ_μ are the Dirac matrices. Eq. (5) ensures the vanishing of the normal component of the fermionic current and scalar densities of quarks at the boundary of the spherical surface:

$$J_n \equiv n_\mu \bar{\psi} \gamma^\mu \psi = 0, \quad \text{and} \quad \bar{\psi} \psi = 0 \quad \text{at} \quad r = R, \quad (6)$$

where \hat{n} is the unit normal four-vector to the boundary. The allowed momentum modes for Eq. (5) are well-known; the relevant equations are given in Appendix A. Then the expression for Ω becomes:

$$\Omega = \frac{(M-m)^2}{4G} - \frac{N_c N_f}{V} \sum_j \sum_{p_{j\kappa}} (2j+1) \left[\left\{ -\frac{\Lambda e^{-\left(\frac{E}{\Lambda}\right)^2}}{\sqrt{\pi}} + E \text{Erfc} \left(\frac{E}{\Lambda} \right) \right\} + T \log \left(1 + e^{-\frac{(E-\mu_q)}{T}} \right) + T \log \left(1 + e^{-\frac{(E+\mu_q)}{T}} \right) \right], \quad (7)$$

where $V = \frac{4}{3}\pi R^3$ is the volume of the system, and $\text{Erfc}(x) = 1 - \frac{2}{\sqrt{\pi}} \int_0^x dy e^{-y^2}$. The term in the curly bracket in Eq. (7) is the vacuum term and the other two terms correspond to the medium quark and antiquark contributions, respectively. M is determined self-consistently from the minimum of Ω : $\frac{\partial \Omega}{\partial M} = 0$. We have used the regulator in the vacuum term only. The medium terms are regulated by temperature and do not need an ultraviolet regulator.

Effects of finite volume on the phase diagram have been explored in the literature in the past. Sometimes the antiperiodic or the periodic boundary conditions have been used for this purpose [15, 18, 19, 22, 31]. Note that these boundary conditions do not capture the finite volume fireball in any way: these are boundary conditions usually imposed in theoretical studies (e.g. numerical studies on the lattice) when the aim is to study the infinite volume system. Besides being easy to implement, the advantage of these boundary conditions is that they show very small deviations from the infinite volume system, and are therefore ideal for studies aiming for the thermodynamic limit. Our purpose here is to estimate the size of the deviation from the infinite volume results due to the finite volume fireball. We do not think (anti)periodic boundary conditions are suitable for this purpose. While the boundary condition Eq. (5), Eq. (6) also do not capture the whole complexity of the finite fireball, we believe it captures the most essential aspects of it and gives a more realistic estimation of the size of the finite volume effects. In Appendix B we compare our results with those of an antiperiodic geometry for a similar system size. We indeed find that the volume effects are much smaller in the antiperiodic geometries.

The finite temperature phase transition is chiral symmetry restoring in nature, and we will track the transition using $\langle\bar{\psi}\psi\rangle$, or equivalently, M . In the absence of the symmetry-breaking term m , in the full quantum theory, the chiral symmetry will be restored in finite volume at all temperatures, due to tunnelling between the classical vacua of $\mathcal{L}_{\text{NJL}}^{\text{MF}}$. In Monte Carlo simulations, this will show an instability in $\langle\bar{\psi}\psi\rangle$. A mean-field treatment will miss the physics of tunnelling, and indicate symmetry breaking at low temperatures. This problem is not there in the presence of the mass term corresponding to physical light quarks, where lattice simulations show a stable result for $\langle\bar{\psi}\psi\rangle$ at quite small volumes down to $m_\pi L \sim 1$.

III. CHIRAL TRANSITION AT FINITE VOLUME

We explore the chiral transition line for Eq. (3), and its shift with volume, for the MIT boundary condition. At $\mu = 0$ the chiral symmetry restoration is a crossover. In Fig. 1, we show the constituent mass, M (Eq. (A1)), which is just a constant shift of $-\langle\bar{\psi}\psi\rangle$ and has the same information as $\langle\bar{\psi}\psi\rangle$. We see a rapid but smooth decrease in M around $T \approx 190$ MeV, indicating a crossover. At low temperatures $\ll T_\chi$, decreasing the volume to $R = 5$ fm decreases the constituent mass by $< 5\%$ from the infinite volume value. At high temperatures > 200 MeV the chiral symmetry is restored and the chiral condensate becomes small. Therefore M becomes small, approaching m . In small-volume systems, the crossover region becomes somewhat smoother, but no qualitative change from the infinite-volume case is seen in systems as small as a 5 fm sphere. This can be further seen in the right panel of Fig. 1, where the derivative dM/dT is shown. To get this plot, we used a cubic spline interpolation of the M vs T data of the left plot. The plot shows a systematic but moderate reduction in the peak height and broadening of the peak, as the volume is reduced. The peak position is an estimate of the crossover temperature T_χ , which changes very slowly with the radius of the sphere, R (a 7 MeV shift from infinite volume to $R = 5$ fm). The chiral susceptibility $\chi_m = -\frac{\partial\langle\bar{\psi}\psi\rangle}{\partial m}$ also shows a peak at the chiral symmetry restoration point. The peak position is close to the peak of dM/dT , though not exactly identical at the crossover region, and the volume dependence is similar to that seen in Fig. 1. Here we will use the peak of dM/dT as our estimate for T_χ . Of course, in the case of a true phase transition (as opposed to a crossover), all these observables will show the same transition temperature.

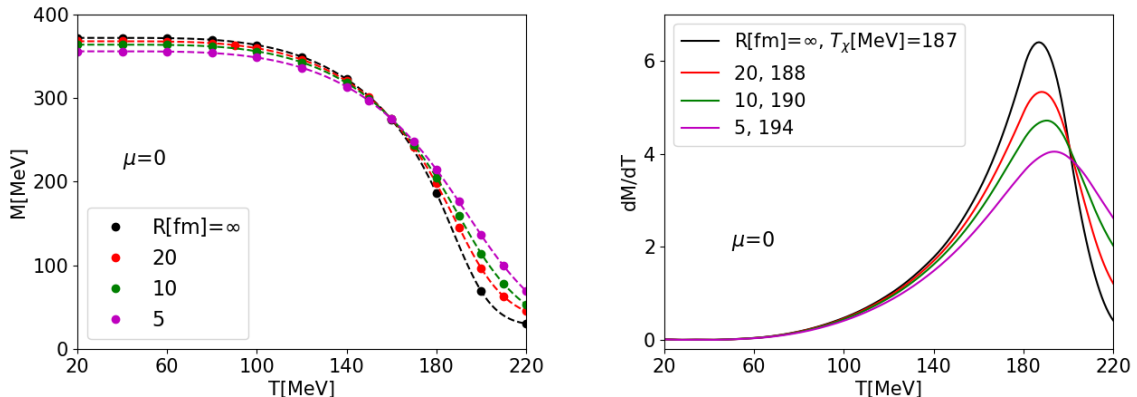


FIG. 1. (Left) Constituent quark mass M as a function of temperature (T) at $\mu = 0$. (Right) The derivative dM/dT . The legend shows the peak position of the dM/dT curves, which can be taken as an estimate of T_χ .

Now we introduce a nonzero quark chemical potential μ . For small values of μ , the qualitative behavior is very similar to what is seen for $\mu = 0$. In Fig. 2, we show M as a function of T at different volumes for three values of μ . The temperature and volume dependence of M at $\mu=100$ MeV is very similar to that at $\mu=0$, as a comparison of the left panel of Fig. 2 with Fig. 1 shows. As μ increases, the crossover shifts to smaller values of temperature, as expected. Also, we find a stiffening of the transition at larger volumes: the smoothing of the transition at small volumes is enhanced. At $\mu=350$ MeV, shown in the right panel of Fig. 2, we find a discontinuity, indicating a first-order transition, at infinite volume. The first-order nature of the transition can be further ascertained by looking at Ω , Fig. 3. At the transition region, a two-minimum structure is seen, which is the hallmark of first-order transition, and indicates phase coexistence. At this μ the transitions are smooth in the finite volume system, even at $R=20$ fm, though at such a large volume it is quite a sharp crossover. We also find here a much more enhanced smoothing of the transition with a reduction of volume: while the curve at $R = 20$ fm indicates a sharp crossover, the one at $R=5$ fm indicates a smooth behavior. Also, the crossover temperature changes much more rapidly here with volume: the transition temperature changes from 47.3 MeV in the infinite volume system to 72.2 MeV in the 5 fm sphere.

Before proceeding with the discussion of the investigation of the transition line at higher μ at finite volume, let us clarify our terminology. In our analysis, the term “first-order transition” corresponds to a two-well structure in the free energy, with well-separated local minima at small and large values of M corresponding to the symmetry restored and symmetry broken phases, respectively. Such a structure will indicate phase coexistence, and possible supercooling/superheating in a dynamical system. This is what we have looked for, and have referred to as the signature of a first-order transition.

In the infinite volume case, tunnelling between the two minima is prohibited. However, in a finite volume, the free energy barrier between the minima is finite, and there is a nonzero probability for tunnelling. This

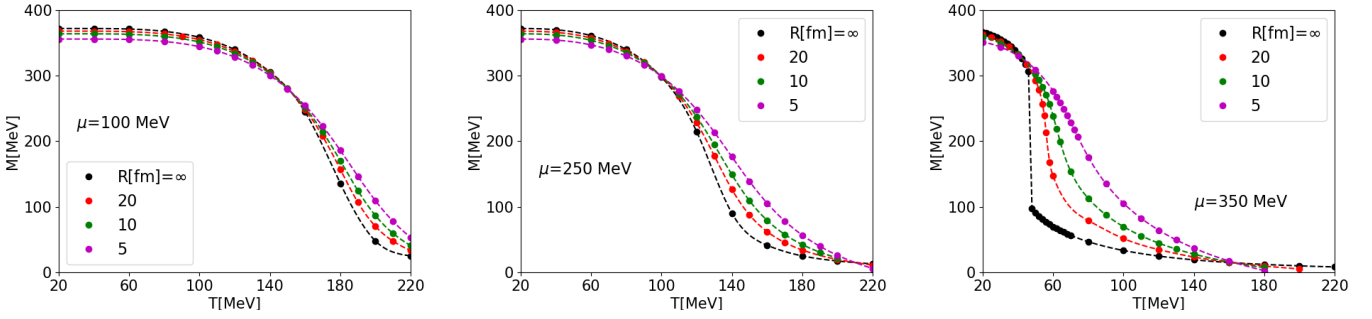


FIG. 2. The dependence of the M vs T curve with volume. Results at $\mu=100$ MeV (left), 250 MeV (middle) and 350 MeV (right) is shown. A discontinuous transition is seen in the infinite volume system at $\mu=350$ MeV.

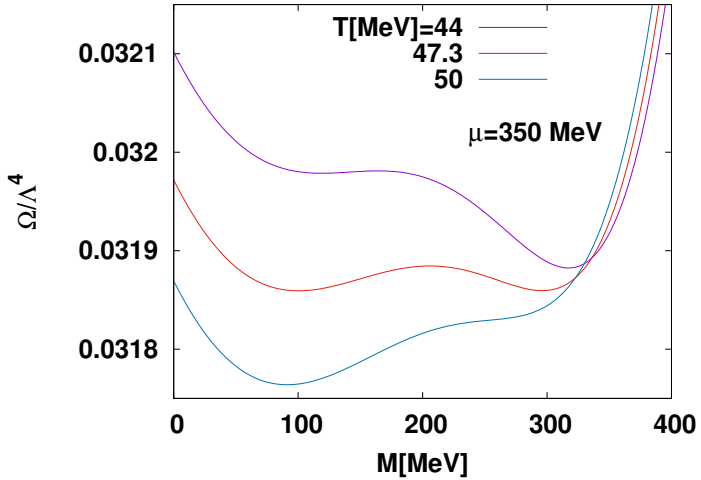


FIG. 3. The thermodynamic potential, $\Omega/\Lambda_{\text{UV}}^4$, in the transition region at $\mu=350$ MeV for an infinite volume system. A small (irrelevant) additive constant $\Omega = \mp 0.0001 \Lambda_{\text{UV}}^4$ has been added to the potentials at $T=44$ and 50 MeV, respectively, for better viewing. The figure indicates a first-order transition at $T \approx 47.3$ MeV.

will lead to a unique minimum at every (T, μ) value for a static system, and strictly speaking, one can only have crossovers in the finite volume system. However, the tunnelling probability is exponentially suppressed in volume. In a fireball which rapidly cools through the transition region, tunnelling will be insignificant unless the volume is very small. In cases where the classical free energy shows a two-minima structure and a discrete jump at the transition, we will expect interesting phenomena, related to the features of a first-order transition, at the transition point (see also Ref.[15]). Therefore, the two-well structure of the mean-field potential, Ω , is of actual physical interest, and we will loosely use terms like first-order line, phase coexistence etc. to refer to such a structure even in a finite volume system. An analysis of the dynamics at discontinuity in a finite volume system has been done in Ref. [32].

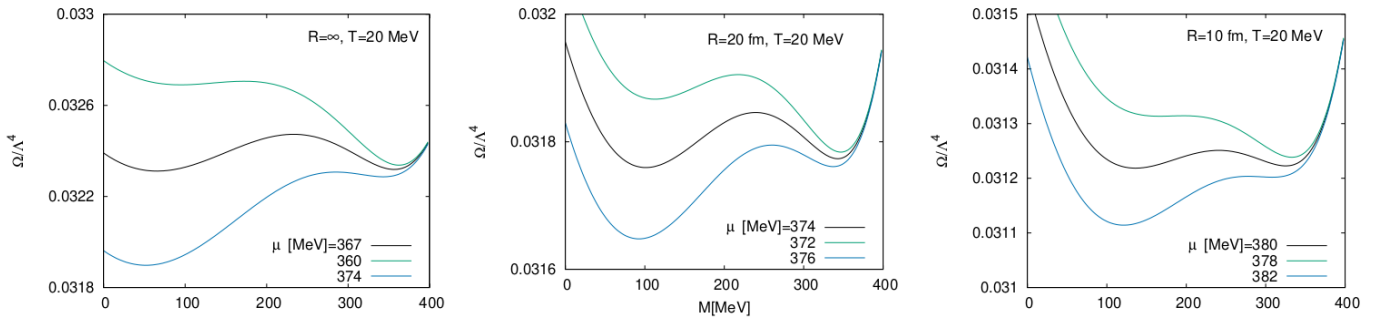


FIG. 4. The mean-field thermodynamic potential in the transition region at $T=20$ MeV for infinite volume (left) and for spheres of radius 20 fm (middle) and 10 fm (right), showing a two-well structure down to a sphere of $R=10$ fm.

We illustrate this behavior in Fig. 4, where we show Ω at different volumes at $T=20$ MeV. We find a two-well structure in Ω even at $R=10$ fm. Note also the range of μ over which this structure is seen (we loosely refer below to this region as the coexistence region). A shift of the transition to higher μ is seen with the reduction in volume; at the same time, a weakening of the double-well structure (and a shrinking of the coexistence region) is seen. At this temperature, we do not find a discontinuous transition in the 5 fm sphere, but as we go further down to $T=0$ we find a discontinuous transition in all our systems.

Our finding of the transition line in the (T, μ) plane is summarized in Fig. 5. The dashed line corresponds to the smooth crossover region, whereas the solid part of the line at small T indicates where the mean field effective potential behaves like a first order transition. We find a shift of the crossover line towards larger values of μ as the system size is reduced. The shift is mild for systems with radii as small as 10 fm, but a more significant shift is seen for the 5 fm sphere.

A more significant volume dependence is found when we investigate the first order transition region at low temperatures. This part is shown more clearly in the inset. As the figure shows, the coexistence region in the mean field potential is pushed down to lower values of T as the system radius is decreased. The dotted lines around the first order line in the inset indicate the estimate of the boundary of the coexistence region. This region shrinks quite strongly as the system size is reduced.

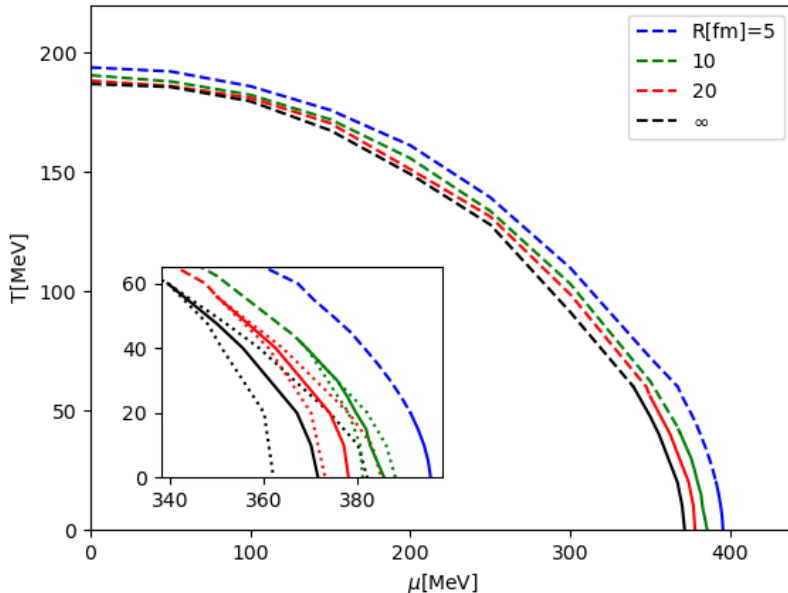


FIG. 5. The shift of the chiral crossover line in the (T, μ) plane with system size. In the inset the large μ part is enlarged, highlighting the first-order region.

IV. NUMBER DENSITY AND QUARK NUMBER SUSCEPTIBILITY

The chiral condensate $\langle \bar{\psi} \psi \rangle$ and, equivalently, the constituent mass M are good order parameters for tracking the chiral transition. They are, however, not directly connected to an experimental observable. The baryon number density (n_B) and susceptibilities of the baryon number operator are, on the other hand, related to experimental observables. In particular, they are of great interest in the large μ_B regime, where one looks for the first order transition line and its endpoint.

At the mean-field level the quark number density ($n = 3n_B$) is simply calculated as

$$n = \frac{\partial P}{\partial \mu} = 2N_c N_f \int \frac{d^3 p}{(2\pi)^3} [n_F(E - \mu; T) - n_F(E + \mu; T)], \quad (8)$$

where n_F is the Fermi distribution, $n_F(x; T) = \left(e^{\frac{x}{T}} + 1 \right)^{-1}$. We start with an investigation of the effect of finite volume on n in the crossover region. In the left panel of Fig. 6, we show the temperature dependence of n at $\mu=100$ MeV. At small values of $\mu \lesssim 100$ MeV, the volume dependence of the number density is small

except in the crossover region ($150 \text{ MeV} \leq T \leq 200 \text{ MeV}$). n is small at small temperatures, and then rises and reaches its asymptotic behavior $\sim \mu T^2$ at high temperatures. In the crossover zone, we see some volume dependence: the rise of n is milder at smaller volumes. This behavior gets further amplified as we go to higher values of μ , where the crossover becomes sharper. In the middle panel of Fig. 6 we show the results for $\mu=250 \text{ MeV}$, still in the crossover region. Since the crossover is now sharper, n increases much more sharply across the transition line at larger volume systems. As we enter the chirally symmetric phase, the temperature is still not sufficiently high to show the asymptotic $\sim \mu T^2$ behavior. As we go to even higher values of μ , we reach the first-order region, where n shows a discontinuous jump across the transition. This is seen in the infinite volume case of the right panel of Fig. 6 ($\mu=350 \text{ MeV}$). The MIT sphere system has a smooth crossover at this value of μ for $R \leq 10 \text{ fm}$, while the 20 fm sphere is close to a transition, as is also seen in Fig. 5. The behavior of n above the transition is quite different at such a large value of μ , as the μ^4 term starts dominating.

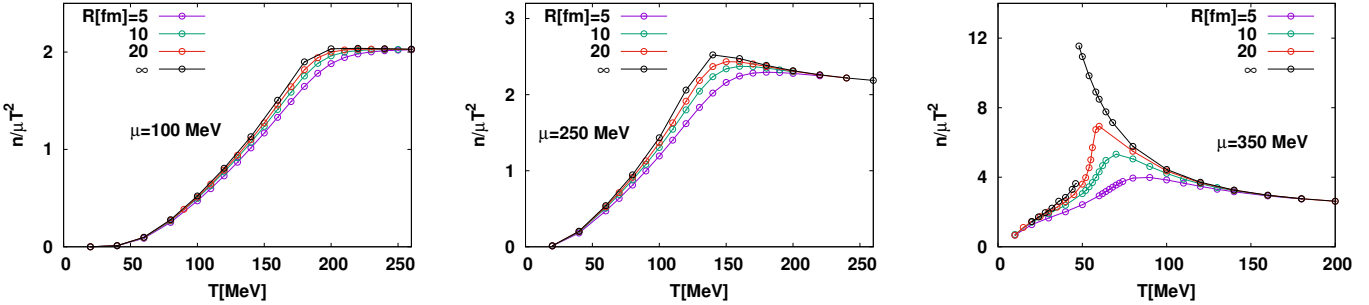


FIG. 6. The quark number density (n) as a function of T on a system of different sizes (with MIT b.c.), at a quark chemical potential μ of 100 MeV (left), 250 MeV (middle) and 350 MeV (right).

The quark number density, and the nonlinear quark number susceptibilities which are higher-order derivatives of the free energy, are very interesting observables, especially for the critical point search. The nonlinear susceptibilities are defined as derivatives of the pressure (P) with respect to the quark chemical potential. Similar susceptibilities of other conserved quantities like charge or strangeness can also be constructed, but here we will concentrate on the quark number susceptibilities or equivalently, baryon number susceptibilities. The k th order susceptibility χ_k is defined as,

$$\chi_k = \frac{\partial^k P}{\partial \mu^k} = \frac{\partial^{k-1} n}{\partial \mu^{k-1}}. \quad (9)$$

The behavior of χ_k can be inferred from the μ dependence of n , as sketched in the left panel of Fig. 7. At a fixed temperature, n increases with μ , with a rapid rise in the transition region. For a sufficiently high temperature $T > T_c$, the critical temperature, one has a crossover. χ_2 therefore shows a moderate peak in this region. As the volume decreases, one expects a smoother crossover; therefore the peak height decreases. This behavior is seen in our calculated χ_2 at different volumes; in the right panel of Fig. 7, we show the results at $\mu = 250 \text{ MeV}$, which is in the crossover region. Note also that the peak position has shifted slightly with volume. This is because of the shift of the crossover line, seen in Fig. 5.

As one goes to lower temperatures, the crossover becomes steeper and eventually one approaches the critical point, where the χ_2 peak is expected to diverge. In Fig. 8 we show χ_2 in the low temperature region of the (T, μ) plane, for MIT spheres with $R=10$ and 5 fm. To obtain the curves, we calculated n_q at a large number of closely spaced values of μ , fitted a cubic spline, and took its derivative. We also checked that the values agreed with χ_2 calculated directly at various points. As we see, the χ_2 peak height increases as one approaches the critical point. As we discussed in Section III, the mean field effective potential shows a critical point also for the finite volume systems. This critical point was seen in Fig. 5 to move to lower temperatures with decreasing volume. The major volume effect seen in Fig. 8 is related to this shift in the critical point with volume. While the critical point in the infinite volume system appears at $T \approx 60 \text{ MeV}$, for the 10 fm sphere one only has a smooth crossover at this temperature. The critical point at this volume shows up at $T \approx 42 \text{ MeV}$, where the height of the χ_2 peak is maximum. At lower temperatures, one has two separate phases at the transition: we calculate χ_2 separately for the two phases, which show moderate values. The end point of the two-state transition happens at an even lower temperature for the 5 fm sphere, shifting the highest χ_2 peak to $T \approx 20 \text{ MeV}$.

It has been suggested [33, 34] that the higher-order susceptibilities are a better probe for the critical region. In particular, χ_3 [35] and χ_4 [36, 37] show very interesting structures in the critical region, and these structures become smoother rapidly with decreasing volume. The behavior of χ_3 across the crossover region has also been sketched in the left panel of Fig. 7. χ_3 has a peak to the lower μ side of the transition line, then changes sign and shows a dip in the higher μ side. These peaks and dips become sharper as one approaches the critical point.

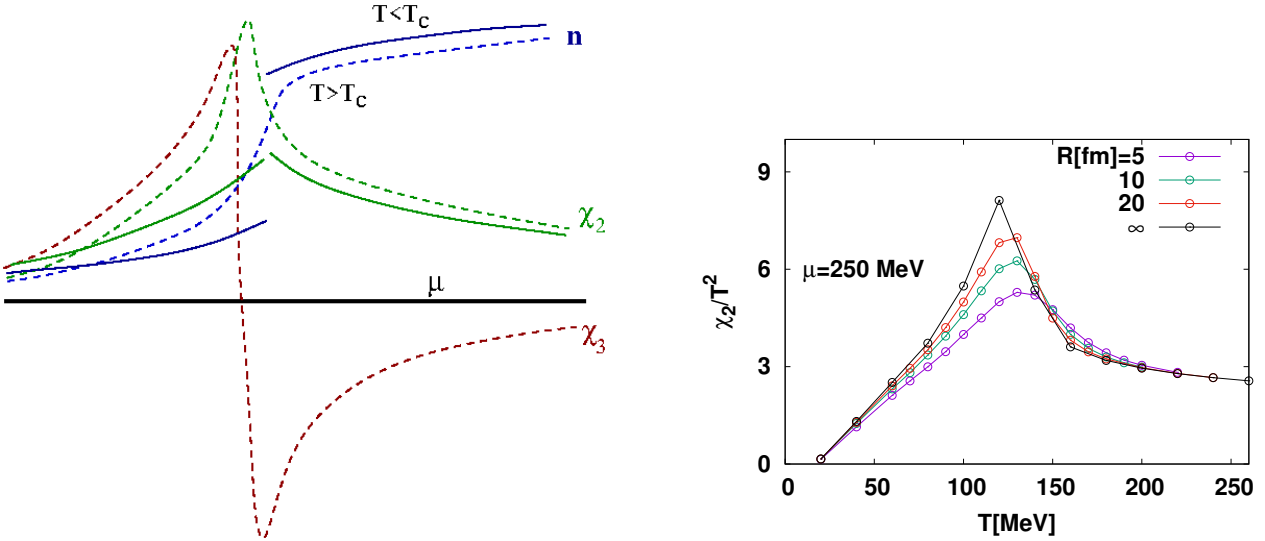


FIG. 7. (Left) Sketch of the μ dependence of the number density n as well as the quark number susceptibilities. The dashed lines show the behavior in the crossover region, at a temperature $T > T_c$, the critical temperature. The solid lines correspond to a temperature $T < T_c$, where one has a first order transition. (Right) The quark number susceptibility χ_2 as a function of T on a system of different sizes (with MIT b.c.), at a quark chemical potential $\mu=250$ MeV, which is in the crossover region.

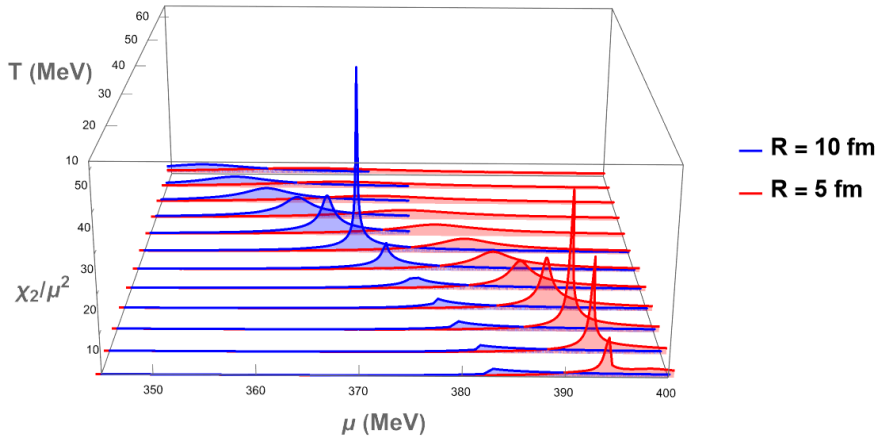


FIG. 8. χ_2 across the chiral transition line for $T \lesssim 60$ MeV, which is the first order transition region for the infinite volume system. Shown are results for spheres of radii 5 and 10 fm.

In the left panel of Fig. 9, we show the contour plot of χ_3 calculated on a 10 fm sphere in the region $40 \leq T \leq 60$ MeV, which is the region between the critical points on 10 fm and infinite volume systems. The qualitative behavior of χ_3 seen in the figure is as sketched in Fig. 7. χ_3 shows a peak as one approaches the transition region from the low μ side, then changes sign at the transition line and takes a large negative value just after the transition line, before becoming small again. The peak height and the valley depth increase as one approaches the critical region for this volume. Note that the structure for the 10 fm sphere is quite mild at $T=60$ MeV, which is close to the critical region for the infinite volume region. Similarly, for the 5 fm sphere, the peak and the valley are mild at $T=40$ MeV (compare the scales), but become steeper as one goes to lower temperatures, towards the endpoint of the discontinuity line for this volume.

In the case of a conventional boundary condition like the antiperiodic one, the shift of the endpoint of first order line is insignificant for a box of size 5 fm or higher (see Appendix B), and the change in the magnitude of the χ_2 peaks are due to the smoother nature of the transition at smaller volumes. As Fig. 8 and Fig. 9 show, here the major effect on the peak structure is due to the shift of the transition point. While our calculation is only at the mean field level, we believe this effect needs to be kept in mind when looking at the volume dependence of the baryon number cumulants (which are closely related to the susceptibilities).

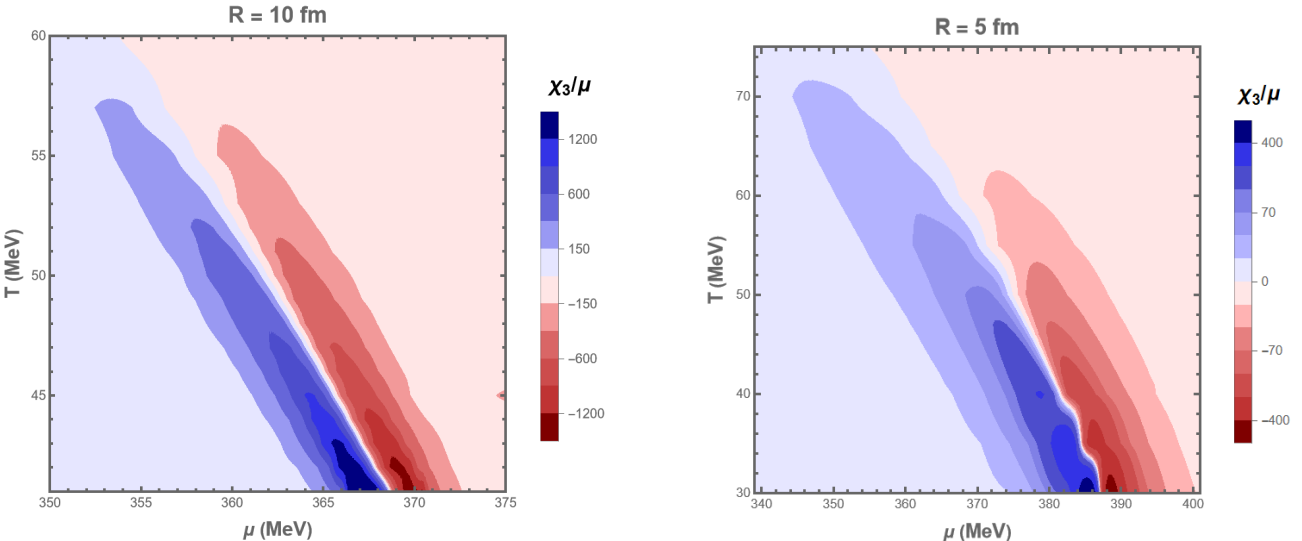


FIG. 9. Contour plots of χ_3/μ near the endpoint of the first order line, for a sphere with a radius of 10 fm(left) and 5 fm (right) with MIT boundary condition. We have used Gaussian filtering to get rid of some spurious local structures which are numerical artifacts.

V. SUMMARY OF RESULTS AND CONCLUSION

The QCD phase diagram has been the subject of intense theoretical and experimental investigation for a few decades. The phases at small values of μ_B and the crossover line are well-understood from non-perturbative numerical studies of QCD using lattice discretization. The phase diagram at large values of μ_B has to be studied using effective models of QCD. In particular, the Nambu Jona-Lasinio model in its different variations has been widely used to study the phase diagram in the (T, μ_B) plane. On the experimental side, the phase diagram is studied by creating a strongly interacting medium at high temperatures and chemical potential in ultrarelativistic heavy ion collisions, in particular, in the BES series of experiments at RHIC, and other planned experiments like the NICA at JINR. To infer the phase diagram from the experiments, it is necessary to compare observables, in particular the number density and its susceptibilities, with theoretical calculations.

The fireball created in the experiments has a finite volume. It is rapidly evolving in time, and its dimensions are a few fermi before freezeout. On the other hand, the theoretical studies are usually for infinite volume, static systems. To infer information about the phase diagram by combining the two, it is therefore important to estimate the effect of the finite size and the dynamic nature of the fireball on the observables studied. In this paper, we have studied one aspect of it, the effect of the finite size of the system. We have studied the 2-flavor NJL model on a sphere, with MIT boundary conditions to mimic the fireball property of having a deconfined medium within the finite volume. While this is an idealization of the complicated geometry of the fireball created in a heavy ion collision, the MIT boundary condition captures the essential feature of the finite volume fireball that the quarks are confined within a finite system. Therefore one can reasonably expect to learn about the effect of the finite size using this setup.

The result of our investigation of the phase diagram can be summarized by Fig. 5, which shows the shift of the transition line with the system volume. For the parameter sets used in our study, the NJL model has a first-order transition line at large μ , ending in a critical point at $(T_c, \mu_c) \approx (60, 340)$ MeV. The actual location of the transition line as well as the endpoint is sensitive to the parameters chosen; the interest of this paper is on the sensitivity of the line on the system volume. Here the transition line has been tracked by the constituent quark mass M , or equivalently, $\langle \bar{\psi} \psi \rangle$. As the figure shows, in the crossover region, the shift of the transition line is mild: even for a system with $R=5$ fm, the shift is only a few MeV. The volume dependence of the number density and its susceptibilities are discussed in Section IV. The volume dependence of the number density and its change across the transition line is shown in Fig. 6. As expected, the change of the number density across the crossover line becomes smoother as the volume is reduced.

The effect of the finite volume on the transition line is more interesting in the first-order region on the high μ side. The first-order region (indicated by the two-minima structure of the mean-field free energy; see Section 3) ends at a lower value of T as the volume is reduced. The number density also shows very similar behavior. The volume dependence is particularly strong in the quark number susceptibilities of the baryon number in the critical region, as seen in Fig. 8. In particular, Fig. 8 shows that the major effect in the variation of the χ_2 peak with volume is due to the shift of the endpoint of the first order line. One expects a sharp peak at

the transition region near this point. As the location of the endpoint shifts with volume, the region of large χ_2 peaks also shifts. This effect seems to be more significant than the expected sharpening of the peak heights with volume. Similarly, χ_3 shows a very interesting behavior across the transition region, with sharp peaks and valleys around the transition line. These structures are seen in Fig. 9 to show an even stronger shift with volume, due to the shift in the location of the critical point. One would expect even larger effects for the higher-order susceptibilities. These results will be relevant for the experimental searches for the critical region, where the critical region is looked for in a small fireball.

VI. ACKNOWLEDGEMENT

A.S. thank Prof. M. Chernodub for a helpful discussion. The computing resources of the Department of Theoretical Physics, TIFR, were used for this work. We would like to thank Ajay Salve and Kapil Ghadiali for their technical assistance. S.D. acknowledges the support of the Department of Atomic Energy, Government of India, under Project Identification No. RTI 4002.

Appendix A: Calculational details

In this section, we give some formulae used in the calculations for obtaining results of Section III and Section IV, and some relevant details.

The chiral condensate causes the quarks to have an effective mass M , and at the mean-field level, the theory can be treated like a Gaussian theory with quarks of mass M . M is calculated self-consistently using the following equations,

$$M = m - 2G \langle \bar{\psi} \psi \rangle, \quad \langle \bar{\psi} \psi \rangle = - \int \mathbb{D}p \text{Tr}[S(p, M)], \quad (\text{A1})$$

where $\mathbb{D}p$ is the regularized four-momentum integral and $S(p, M)$ is the free quark propagator matrix.

We work with the proper time regularization, in which the momentum regulator is imposed as,

$$\frac{1}{p^2 + M^2} \longrightarrow \int_{\tau_{\text{UV}}=1/\Lambda_{\text{UV}}^2}^{\infty} d\tau e^{-\tau(p^2 + M^2)}, \quad (\text{A2})$$

and we get the chiral condensate,

$$\langle \bar{\psi} \psi \rangle = -4N_c N_f M \int \frac{d^4 p}{(2\pi)^4} \int_{\tau_{\text{UV}}}^{\infty} d\tau e^{-\tau(p^2 + M^2)} = -\frac{N_f N_c M}{4\pi^2} \int_{\tau_{\text{UV}}}^{\infty} \frac{d\tau}{\tau^2} e^{-M^2 \tau}. \quad (\text{A3})$$

We can easily isolate the terms quadratic and logarithmic in Λ_{UV} :

$$\langle \bar{\psi} \psi \rangle = -\frac{N_f N_c M^3}{4\pi^2} \left(\frac{\Lambda_{\text{UV}}^2}{M^2} e^{-M^2/\Lambda_{\text{UV}}^2} - \Gamma \left(0, \frac{M^2}{\Lambda_{\text{UV}}^2} \right) \right), \quad \Gamma(0, x) = -\gamma - \log x - \sum_{k=1}^{\infty} \frac{(-x)^k}{k \cdot k!}, \quad (\text{A4})$$

where $\Gamma(0, x)$ is the incomplete Gamma function, and $\gamma \approx 0.577$ is the Euler's constant [38].

\mathcal{L}_{NJL} is a non-renormalizable theory, and the results depend on Λ_{UV} . A comparison of various regularization schemes can be found in Ref. [28]. In particular, the result for $\langle \bar{\psi} \psi \rangle$ in dimensional regularization with \overline{MS} scheme is,

$$\langle \bar{\psi} \psi \rangle_{\overline{MS}} = -\frac{N_f N_c M^3}{4\pi^2} \left(-1 - \log \frac{\bar{\mu}^2}{M^2} \right), \quad (\text{A5})$$

where $\bar{\mu}$ is the \overline{MS} scale, and we have done the standard \overline{MS} subtraction $\frac{1}{\epsilon} - \gamma + \log(4\pi)$ from the right hand side of Eq. (A5). If we were to do the standard renormalization prescription of taking $\Lambda_{\text{UV}} \rightarrow \infty$ in Eq. (A4), then matching to Eq. (A5) would require a subtraction of

$$-\frac{N_f N_c M}{4\pi^2} \left[\Lambda_{\text{UV}}^2 + M^2 \left(\log \frac{\bar{\mu}^2}{\Lambda_{\text{UV}}^2} + \gamma \right) \right]$$

at this order. Of course, we keep Λ_{UV} finite, and the results depend on the details of the regularization.

At finite temperature, the integral over p_0 gets replaced by a sum over the Matsubara modes $(2n+1)\pi T$, leading to the mean-field result for the thermodynamic potential:

$$\Omega = \frac{(M-m)^2}{4G} - 2N_c N_f \int \frac{d^3 p}{(2\pi)^3} \left[\left\{ -\frac{\Lambda e^{-\left(\frac{E}{\Lambda}\right)^2}}{\sqrt{\pi}} + E \operatorname{Erfc}\left(\frac{E}{\Lambda}\right) \right\} + T \log\left(1 + e^{-\frac{(E-\mu_q)}{T}}\right) + T \log\left(1 + e^{-\frac{(E+\mu_q)}{T}}\right) \right]. \quad (\text{A6})$$

The chiral condensate becomes:

$$\langle \bar{\psi} \psi \rangle(T, \mu) = -\frac{N_f N_c M}{4\pi^2} \left[\int_{\tau_{\text{UV}}}^{\infty} \frac{d\tau}{\tau^2} e^{-M^2 \tau} - \frac{1}{E_p} (n_F(E_p - \mu; T) + n_F(E_p + \mu; T)) \right], \quad (\text{A7})$$

where $E_p = \sqrt{p^2 + M^2}$. Note that we have only regularized the vacuum term, as the terms with the Fermi distributions are already regularized by the temperature scale.

The momentum modes for the MIT boundary condition on a sphere can be obtained by solving the Dirac equation for fermions of mass M and imposing the MIT boundary condition Eq. (5) on the eigenfunction. The allowed momentum modes satisfy the condition [13],

$$j_{l_\kappa}(pR) = -\operatorname{sign}(\kappa) \left(\frac{p}{E + M} \right) j_{l_{\bar{\kappa}}}(pR). \quad (\text{A8})$$

Here, j_l is l^{th} order spherical Bessel function, and

$$l_\kappa = \begin{cases} -\kappa - 1 & \text{for } \kappa < 0 \\ \kappa & \text{for } \kappa > 0 \end{cases} \quad (\text{A9})$$

$$l_{\bar{\kappa}} = \begin{cases} -\kappa & \text{for } \kappa < 0 \\ \kappa - 1 & \text{for } \kappa > 0. \end{cases} \quad (\text{A10})$$

The energy eigenvalue for such a system is,

$$E \equiv E_{\kappa, i} = \sqrt{q_{\kappa, i}^2 + M^2}, \quad (\text{A11})$$

where $q_{\kappa, i} \equiv pR$ is obtained by solving Eq. (A8). Here, i is the radial excitation quantum number ($i = 1, 2, 3, \dots$) and $\kappa = \pm(j + 1/2)$ is for the total angular momentum, $j = 1/2, 3/2, \dots$. Replacing the three-momentum integral in Eq. (A6) by a sum over these modes leads to Eq. (7).

Appendix B: Comparison with other boundary conditions

The QCD phase diagram at finite volume has been studied in the literature, using the NJL model [24, 39] and other effective models like the PNJL [16, 17], the linear sigma and the Polyakov quark-meson model [15, 20, 40], etc., as well as using the Dyson-Schwinger equation [31] and the functional renormalization group [18]. As we have mentioned in Section II, most of the studies have used the periodic (PBC) or the antiperiodic (APBC) boundary condition. For a cubic box of volume L^3 , they correspond to momentum sum with spatial momenta $\frac{2n\pi}{L}$ and $\frac{(2n+1)\pi}{L}$, respectively. Also in some works [16, 17, 20], an infrared cutoff $\frac{\pi}{L}$ has been used in the momentum integral to mimic a system of dimensions L , but the geometry has not been specified. As we have mentioned in Section II, we do not think such boundary conditions mimic the finite size of the fireball. The MIT boundary condition used here captures the essential physics, though in a very simplified form, of the finite-size fireball.

To see how much the results with the MIT boundary condition differ from the other boundary conditions, we have compared the size of the finite volume effects with the different boundary conditions, by looking at the constituent mass M . In the left panel of Fig. 10, we have compared the results for the temperature dependence of M at $\mu = 0$ for APBC and the IR cutoff for a box of dimension $L=5$ fm, with those obtained for a sphere with $R=5$ fm with MIT boundary condition.

As anticipated in Section II, the finite volume effect is significantly larger with the MIT boundary than what is seen with the other boundary conditions. The APBC and the IR momentum cutoff show very little deviation from the infinite volume result even at $L=5$ fm. The PBC is expected to show even less finite volume effect than the APBC, as has been seen in lattice studies. In the chiral symmetry broken phase, the finite volume effect with the MIT boundary condition on a sphere is clearly more than that with APBC and IR cutoff, despite the

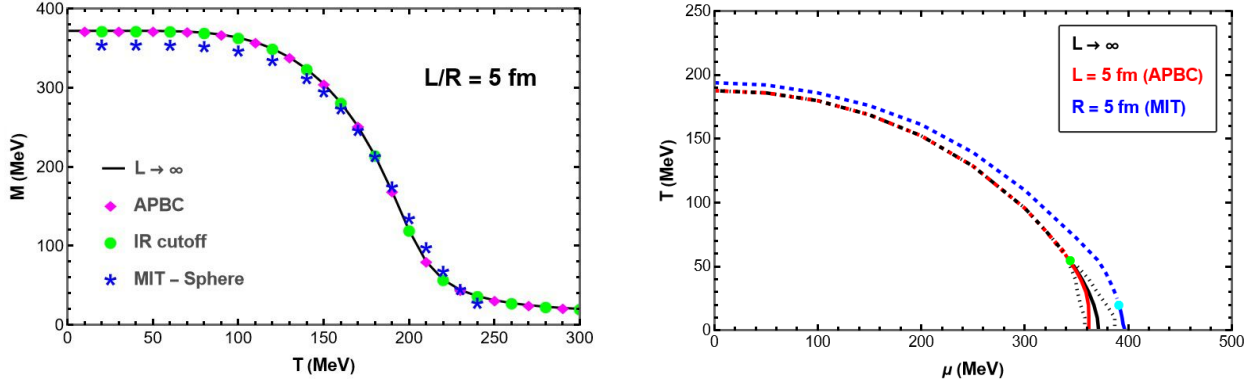


FIG. 10. (Left) Constituent quark mass (M) as a function of temperature (T) at $\mu = 0$ for different boundary conditions. (Right) The transition/crossover line in the (T, μ) plane for a small system with MIT and antiperiodic boundary conditions, compared with the infinite volume line. In both these figures the MIT boundary condition is imposed on a sphere with radius $R = 5$ fm, while the other boundary conditions use a cubic box with side $L = 5$ fm.

volume of the sphere being about four times larger than those with a cubic geometry. In the high-temperature symmetry restored phase the boundary effect is substantially smaller for all the boundary conditions.

In the right panel of the figure, we have compared the phase transition line in the (T, μ) plane for an infinite volume system, along with those obtained for a finite volume box of dimension 5 fm with APBC and a sphere of radius 5 fm with MIT boundary condition. The interpretation of the line is similar to that used in Section III and in Fig. 5: it is the line obtained from the M dependence of the mean field effective potential. The antiperiodic box shows very little volume dependence even at 5 fm: the crossover line is very close to the infinite volume one, and even the coexistence region in M starts to appear at a very similar values of (T, μ) [41]. At lower temperatures, the “first order line” (in the mean field effective potential sense) shows slight deviation from the infinite volume case, but still within the coexistence region. On the other hand, as discussed in Section III, the MIT boundary condition leads to a substantial change: the crossover line is pushed to higher values of μ at all temperatures. Also the coexistence region is shrunk significantly at this volume. Fig. 10 supports our intuition that the studies with the APBC and similar boundary conditions significantly underestimate the finite volume effect. While the APBC and the PBC are not suitable for studying the finite volume fireball, they

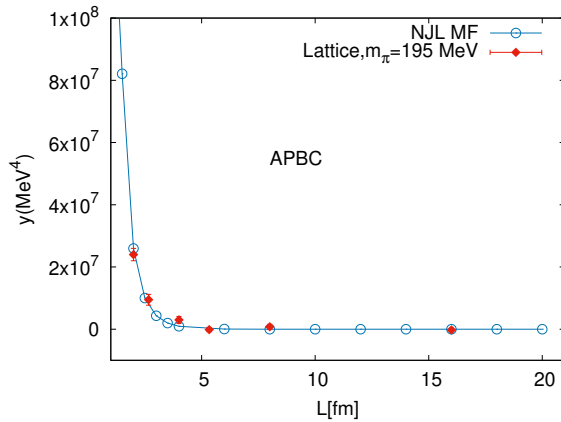


FIG. 11. Comparison of y , Eq. (B1), between lattice and MF NJL with APBC.

are excellent for numerical lattice studies, where one tries to get the infinite volume results from simulations on finite boxes. These boundary conditions are easy to implement on lattice, and show very little volume effect, making it easy to extrapolate to infinite volume from relatively small boxes. To check whether the mean-field NJL model qualitatively captures the volume dependence of the chiral condensate, we compared the results from lattice for $\langle \bar{\psi} \psi \rangle$ on small boxes with the NJL MF results. $\langle \bar{\psi} \psi \rangle$ is regularization dependent; in principle, one can use results like those in Appendix A to compare the results from different regularizations. Instead, we for simplicity compared the renormalization group invariant quantity:

$$y = m [\langle \bar{\psi} \psi \rangle(L) - \langle \bar{\psi} \psi \rangle(L \rightarrow \infty)]. \quad (B1)$$

The result of such a comparison is shown in Fig. 11. This is a qualitative comparison where the lattice pion is somewhat heavier (≈ 200 MeV). Also for the lattice, the $L \rightarrow \infty$ is replaced by the largest lattice we used. So a precise agreement is not expected. But as Fig. 11 shows, the deviation from the full theory at a very small volume is qualitatively captured in the NJL MF result. This gives us hope that the results we obtained for the MIT boundary condition, despite the many caveats, qualitatively capture the trend of the finite volume effect of a static fireball.

[1] The ALICE experiment – A journey through QCD, (2022), arXiv:2211.04384 [nucl-ex].
 [2] M. Arslandok *et al.*, Hot QCD White Paper, (2023), arXiv:2303.17254 [nucl-ex].
 [3] M. J. Tannenbaum, Highlights from BNL-RHIC, *Subnucl. Ser.* **49**, 295 (2013), arXiv:1201.5900 [nucl-ex].
 [4] L. Adamczyk *et al.* (STAR), Bulk Properties of the Medium Produced in Relativistic Heavy-Ion Collisions from the Beam Energy Scan Program, *Phys. Rev. C* **96**, 044904 (2017), arXiv:1701.07065 [nucl-ex].
 [5] G. Aarts *et al.*, Phase Transitions in Particle Physics: Results and Perspectives from Lattice Quantum Chromodynamics, *Prog. Part. Nucl. Phys.* **133**, 104070 (2023), arXiv:2301.04382 [hep-lat].
 [6] P. Braun-Munzinger, V. Koch, T. Schäfer, and J. Stachel, Properties of hot and dense matter from relativistic heavy ion collisions, *Phys. Rept.* **621**, 76 (2016), arXiv:1510.00442 [nucl-th].
 [7] D. Blaschke, Recent selected theory developments for NICA, *EPJ Web Conf.* **138**, 01004 (2017), arXiv:1702.00129 [nucl-th].
 [8] D. Almaalol *et al.*, QCD Phase Structure and Interactions at High Baryon Density: Continuation of BES Physics Program with CBM at FAIR, (2022), arXiv:2209.05009 [nucl-ex].
 [9] A. Lovato *et al.*, Long Range Plan: Dense matter theory for heavy-ion collisions and neutron stars, (2022), arXiv:2211.02224 [nucl-th].
 [10] M. Buballa, NJL model analysis of quark matter at large density, *Phys. Rept.* **407**, 205 (2005), arXiv:hep-ph/0402234.
 [11] K. Fukushima, Chiral effective model with the Polyakov loop, *Phys. Lett. B* **591**, 277 (2004), arXiv:hep-ph/0310121.
 [12] R. L. Jaffe and A. Manohar, BOUND STATES OF THE DIRAC EQUATION OUTSIDE A HARD SPHERE, *Annals Phys.* **192**, 321 (1989).
 [13] W. Greiner and A. Schaefer, *Quantum chromodynamics* (1995).
 [14] H. T. Elze and W. Greiner, Finite Size Effects for Quark - Gluon Plasma Droplets, *Phys. Lett. B* **179**, 385 (1986).
 [15] L. F. Palhares, E. S. Fraga, and T. Kodama, Chiral transition in a finite system and possible use of finite size scaling in relativistic heavy ion collisions, *J. Phys. G* **38**, 085101 (2011), arXiv:0904.4830 [nucl-th].
 [16] A. Bhattacharyya, P. Deb, S. K. Ghosh, R. Ray, and S. Sur, Thermodynamic Properties of Strongly Interacting Matter in Finite Volume using Polyakov-Nambu-Jona-Lasinio Model, *Phys. Rev. D* **87**, 054009 (2013), arXiv:1212.5893 [hep-ph].
 [17] A. Bhattacharyya, R. Ray, and S. Sur, Fluctuation of strongly interacting matter in the Polyakov–Nambu–Jona–Lasinio model in a finite volume, *Phys. Rev. D* **91**, 051501 (2015), arXiv:1412.8316 [hep-ph].
 [18] G. Almasi, R. Pisarski, and V. Skokov, Volume dependence of baryon number cumulants and their ratios, *Phys. Rev. D* **95**, 056015 (2017), arXiv:1612.04416 [hep-ph].
 [19] B. Klein, Modeling Finite-Volume Effects and Chiral Symmetry Breaking in Two-Flavor QCD Thermodynamics, *Phys. Rept.* **707-708**, 1 (2017), arXiv:1710.05357 [hep-ph].
 [20] N. Magdy, Influence of Finite Volume Effect on the Polyakov Quark–Meson Model, *Universe* **5**, 94 (2019), arXiv:1904.10949 [nucl-th].
 [21] J. Bernhardt, C. S. Fischer, and P. Isserstedt, Finite-volume effects in baryon number fluctuations around the QCD critical endpoint, *Phys. Lett. B* **841**, 137908 (2023), arXiv:2208.01981 [hep-ph].
 [22] G. Kovács, P. Kovács, G. Wolf, P. M. Lo, and K. Redlich, Sensitivity of finite size effects to the boundary conditions and the vacuum term, *Phys. Rev. D* **108**, 076010 (2023), arXiv:2307.10301 [hep-ph].
 [23] G. Kovács, P. Kovács, P. M. Lo, K. Redlich, and G. Wolf, Finite volume effects in the extended linear sigma model via low momentum cutoff, *PoS FAIRness2022*, 029 (2023), arXiv:2302.12925 [hep-ph].
 [24] Z. Zhang, C. Shi, and H. Zong, Nambu–Jona–Lasinio model in a sphere, *Phys. Rev. D* **101**, 043006 (2020), arXiv:1908.08671 [hep-ph].
 [25] M. N. Chernodub and S. Gongyo, Interacting fermions in rotation: chiral symmetry restoration, moment of inertia and thermodynamics, *JHEP* **01**, 136, arXiv:1611.02598 [hep-th].
 [26] M. N. Chernodub and S. Gongyo, Effects of rotation and boundaries on chiral symmetry breaking of relativistic fermions, *Phys. Rev. D* **95**, 096006 (2017), arXiv:1702.08266 [hep-th].
 [27] S. P. Klevansky, The Nambu–Jona–Lasinio model of quantum chromodynamics, *Rev. Mod. Phys.* **64**, 649 (1992).
 [28] H. Kohyama, D. Kimura, and T. Inagaki, Regularization dependence on phase diagram in Nambu–Jona–Lasinio model, *Nucl. Phys. B* **896**, 682 (2015), arXiv:1501.00449 [hep-ph].
 [29] A. Bazavov *et al.* (HotQCD), Chiral crossover in QCD at zero and non-zero chemical potentials, *Phys. Lett. B* **795**, 15 (2019), arXiv:1812.08235 [hep-lat].
 [30] D. A. Clarke, P. Dimopoulos, F. Di Renzo, J. Goswami, C. Schmidt, S. Singh, and K. Zambello, Searching for the QCD critical endpoint using multi-point Padé approximations, (2024), arXiv:2405.10196 [hep-lat].
 [31] J. Bernhardt, C. S. Fischer, P. Isserstedt, and B.-J. Schaefer, Critical endpoint of QCD in a finite volume, *Phys. Rev. D* **104**, 074035 (2021), arXiv:2107.05504 [hep-ph].
 [32] E. S. Fraga and R. Venugopalan, Finite size effects on nucleation in a first order phase transition, *Physica A* **345**,

121 (2004), arXiv:hep-ph/0304094.

[33] M. A. Stephanov, Non-Gaussian fluctuations near the QCD critical point, *Phys. Rev. Lett.* **102**, 032301 (2009), arXiv:0809.3450 [hep-ph].

[34] S. Gupta, Finding the critical end point of QCD: Lattice and experiment, *PoS CPOD2009*, 025 (2009), arXiv:0909.4630 [nucl-ex].

[35] M. Asakawa, S. Ejiri, and M. Kitazawa, Third moments of conserved charges as probes of QCD phase structure, *Phys. Rev. Lett.* **103**, 262301 (2009), arXiv:0904.2089 [nucl-th].

[36] R. V. Gavai and S. Gupta, Lattice QCD predictions for shapes of event distributions along the freezeout curve in heavy-ion collisions, *Phys. Lett. B* **696**, 459 (2011), arXiv:1001.3796 [hep-lat].

[37] M. A. Stephanov, On the sign of kurtosis near the QCD critical point, *Phys. Rev. Lett.* **107**, 052301 (2011), arXiv:1104.1627 [hep-ph].

[38] I. S. Gradshteyn and I. M. Ryzhik, *Table of Integrals, Series, and Products* (1943).

[39] Q. Wang, Y. Xiq, and H. Zong, Nambu–Jona-Lasinio model with proper time regularization in a finite volume, *Mod. Phys. Lett. A* **33**, 1850232 (2018), arXiv:1806.05315 [hep-ph].

[40] S. Pal, A. Motornenko, V. Vovchenko, A. Bhattacharyya, J. Steinheimer, and H. Stoecker, Effect of finite volume on thermodynamics of quark-hadron matter, (2023), arXiv:2306.10596 [hep-ph].

[41] For the linear sigma model, a significant shift of the transition line, and shift of the endpoint of the first order line towards lower temperatures, have been reported for a 5 fm box with APBC and PBC [15].